

Stochastic transport theory for investigating the three-dimensional canopy structure from space measurements

Dong Huang^{a,*}, Yuri Knyazikhin^a, Weile Wang^a, Donald W. Deering^b, Pauline Stenberg^c, Nikolay Shabanov^a, Bin Tan^a, Ranga B. Myneni^a

^a Department of Geography, Boston University, 675 Commonwealth Avenue, Boston, MA 02215, USA

^b NASA's Goddard Space Flight Center, Greenbelt, Maryland, 20771, USA

^c Department of Forest Ecology, University of Helsinki, FI-00014, Finland

Received 19 December 2005; received in revised form 28 April 2006; accepted 4 May 2006

Abstract

Radiation reflected from vegetation canopies exhibits high spatial variation. Satellite-borne sensors measure the *mean* intensities emanating from heterogeneous vegetated pixels. The theory of radiative transfer in stochastic media provides the most logical linkage between satellite observations and the three-dimensional canopy structure through a closed system of simple equations which contains the *mean* intensity and higher statistical moments directly as its unknowns. Although this theory has been a highly active research field in recent years, its potential for satellite remote sensing of vegetated surfaces has not been fully realized because of the lack of models of a canopy pair-correlation function that the stochastic radiative transfer equations require. The pair correlation function is defined as the probability of finding simultaneously phytoelements at two points. This paper presents analytical and Monte Carlo generated pair correlation functions. Theoretical and numerical analyses show that the spatial correlation between phytoelements is primarily responsible for the effects of the three-dimensional canopy structure on canopy reflective and absorptive properties. The pair correlation function, therefore, is the most natural and physically meaningful measure of the canopy structure over a wide range of scales. The stochastic radiative transfer equations naturally admit this measure and thus provide a powerful means to investigate the three-dimensional canopy structure from space. Canopy reflectances predicted by the stochastic equations are assessed by comparisons with the PARABOLA measurements from coniferous and broadleaf forest stands in the BOREAS Southern Study Areas. The pair correlation functions are derived from data on tree structural parameters collected during field campaigns conducted at these sites. The simulated canopy reflectances compare well with the PARABOLA data.

© 2007 Elsevier Inc. All rights reserved.

Keywords: Stochastic radiative transfer; 3D canopy structure

1. Introduction

The three-dimensional (3D) structure of vegetation canopies determines the spatial distribution of intercepted solar radiation which drives various physiological and physical processes integral to the functioning of plants. Thus, monitoring of the 3D canopy structure has long been one of the main goals of vegetation remote sensing from space (Castel et al., 2001; Diner et al., 1999; Justice et al., 1998; Ranson et al., 1997). The

3D radiative transfer theory provides the most logical linkage between satellite observations and the physics of processes operative in the generation of signals in optical remote sensing data (Davis & Knyazikhin, 2005; Knyazikhin et al., 2005a). Its direct use in *operational data processing*, however, is not feasible because of high computational costs. Therefore, the use of one-dimensional (1D) models is still the preferred option. The success of remote sensing of vegetation, thus, depends on being able to develop a radiative transfer approach for modeling the radiation regime of natural vegetation which is as realistic as the 3D model and as simple as the 1D model.

At a given spatial location, the vegetation canopy should be treated as a realization of a 3D random field. Satellite-borne sensors measure the *mean radiation field* emanating from a satellite pixel.

* Corresponding author. Current affiliation: Environmental Sciences Department, Brookhaven National Laboratory, 75 Rutherford Dr., Upton, NY 11973. Tel.: +1 631 344 5818; fax: +1 631 344 2887.

E-mail address: dhuang@bnl.gov (D. Huang).

The interpretation of satellite observations requires an accurate specification of relationships between statistical characteristics of the 3D vegetation canopy and the corresponding characteristics of the 3D radiation field. Conceptually, their derivation is straightforward (Pomraning, 1991). One generates from the presumed known statistics of the vegetation canopy a certain realization of the 3D vegetation in a satellite pixel. For this realization, the 3D canopy radiation field is evaluated, either using a 3D canopy radiation model or by a Monte Carlo procedure. One repeats this process for all possible statistical realizations of the canopy, and then averages the corresponding radiation fields to obtain the ensemble average signature and higher statistical moments.

Most of existing canopy-radiation models, however, use “non-stochastic” approaches to build angular and/or spectral signatures of vegetation. In terms of the above straightforward procedure, one first averages the canopy structure and then solves the radiative transfer problem with average characteristics. As it is illustrated in Fig. 1, the use of the stochastic and non-stochastic approaches can result in different relationships between mean characteristics of canopy structure and canopy-leaving radiation. In this simple example, the stochastic approach has captured two important effects of the 3D canopy structure on the relationship between leaf area index (LAI) and canopy reflectance while the conventional approach has not; that is, the reflectance saturation occurs at a higher LAI and the canopy reflectance at red

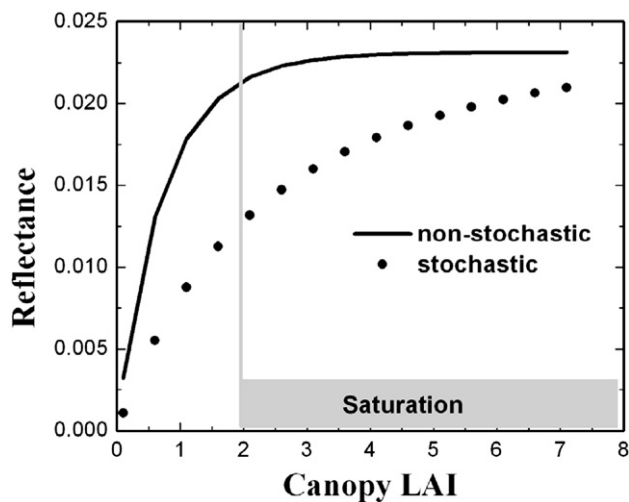


Fig. 1. Hemispherical reflectance at red wavelength as a function of the canopy leaf area index (LAI) calculated using (1) stochastic (dots) and (2) non-stochastic (solid line) approaches. Calculations are performed for a vegetation canopy consisting of identical cylindrical in shape trees uniformly distributed in a pixel bounded from below by a non-reflecting surface. The 3D canopy structure is parameterized in terms of the leaf area index of an individual tree, L_0 , crown radius, r , and crown height, H . The number of trees, m , in the pixel is a random variable distributed according to the Poisson distribution with the parameter \bar{m} (the mean value of m). In the first case, for a given value of \bar{m} , the canopy reflectance, ground cover, g , and canopy LAI (gL_0) were calculated for each realization of m first and then averaged over all realizations. The ensemble average reflectance satisfies the stochastic 1D radiative transfer equations (Appendix A). In the second case, the relationship was obtained by deriving the ensemble average canopy LAI first and then solving the radiative transfer problem using the average canopy LAI as input. The canopy reflectance coincides with the solution of the conventional 1D radiative transfer equations (Appendix B). Canopy structural parameters are set as follows: $L_0=10$, $H=1$, $r=0.5$. The mean number of trees, \bar{m} , is variable.

wavelength is lower than the conventional approach predicts (Asrar et al., 1992; Shabanov et al., 2005).

The theory of radiative transfer in stochastic media aims at deriving a closed system of simple equations which contains the ensemble-average intensity directly as one of its unknowns (Pomraning, 1991, 1996). Since satellite-borne sensors measure the mean intensities reflected from heterogeneous vegetated pixels, we will use the stochastic 1D radiative transfer equations to compute the horizontally averaged 3D radiation fields (Kotchenova et al., 2003; Shabanov et al., 2000; Vainikko, 1973). Their computational cost is comparable to that of the conventional 1D radiative transfer equation.

Radiative transfer in stochastic media has been a highly active research field in recent years (Byrne, 2005; Pomraning, 1991, 1996). The first significant and successful attempt to derive a closed system of equations for statistical characteristics of the 3D radiation field in cloudy atmosphere was made by Vainikko (1973) and later by Titov (1990). Shabanov et al. (2000) adapted these equations to examine the radiation regime in discontinuous vegetation canopies. It was demonstrated that a complete description of statistical characteristics of the 3D canopy radiation regime is possible, using not only average values of radiation over the canopy space, but also averages over space occupied by absorbing elements. A new equation for canopy absorption, which extends the equation for a homogeneous case, was obtained for the general case of discontinuous media. These results were partly implemented to operationally produce LAI and fraction of absorbed photosynthetically active radiation (FPAR) from MODIS (Collection 5) and MISR (version 3.3) data (Shabanov et al., 2005). However, the potential of the theory for remote sensing of vegetation canopies has not been fully realized because of the lack of statistical models of a leaf pair-correlation function that the stochastic transport equations require (Kotchenova et al., 2003). The aim of the present paper is to develop such models, to demonstrate the ability of the stochastic radiative transfer to capture 3D effects, and to assess its validity by comparing simulation results with field data.

The paper is organized as follows. Section 2, Appendices A and B introduce the basic definitions and equations of the stochastic transport theory. Monte Carlo generated and analytical models of the pair correlation function and its properties are discussed in Section 3 and Appendix C. The ability of the stochastic radiative transfer equation to reproduce 3D effects reported in literature is illustrated in Section 4. Evaluation of the stochastic approach with field data is presented in Section 5. Finally, Section 6 summarizes the results.

2. Vegetation canopy as a stochastic medium

Consider a vegetation canopy confined to $0 < z < H$. The plane surfaces $z=0$ and $z=H$ constitute its upper and lower boundaries, respectively. For ease of analysis, we ignore all organs other than green leaves. We will adopt a stochastic view of the landscape and its spatial structure proposed by Jupp et al. (1988). In a given area, the vegetation canopy is a realization of a stochastic process of space. We describe the 3D canopy structure with the indicator function $\gamma(r)$ whose value is 1, if there is a leaf in a volume element

about the spatial point $r=(x, y, z)$, and 0 otherwise (Knyazikhin et al., 1998a, 2005b). Since the vegetation canopy is treated as a stochastic medium, the indicator function is a stochastic function of space. It provides the most general description of the canopy structure that accounts for both its macroscale (e.g., dimensions of trees and their spatial distribution) and microscale (e.g., the clumping of leaves into tree crown) properties.

Each foliated point is characterized by the leaf area volume density d_L (in m^2/m^3) defined as the expectation of the one-sided leaf area in a unit volume with leaves (Kotchenova et al., 2003; Shabanov et al., 2000). This definition means that the leaf area in a volume element dr is either zero or $d_L dr$. The distribution of the leaf area is given by the leaf area density distribution function $u_L(r)=d_L \gamma(r)$ (in m^2/m^3) which is a stochastic function of space. The 3D leaf area density distribution function along with the leaf normal distribution function and the leaf scattering phase function are required to specify coefficients in the deterministic 3D radiative transfer equation (Knyazikhin et al., 2005a; Myneni, 1991; Ross, 1981) which underlies the derivation of the system of stochastic equation (Appendix A). The latter two variables are assumed to be deterministic and independent on the spatial variable r .

Given a realization of the canopy structure, $\gamma(r)$, the corresponding realization of the canopy radiation field is described by the deterministic 3D transport equation. Its solution is the monochromatic intensity, $I_\gamma(r, \Omega)$, which depends on wavelength, location $r=(x, y, z)$ and direction Ω . Statistical characteristics of the canopy radiation field can be determined by averaging realizations of $I_\gamma(x, y, z, \Omega)$. Our aim is to obtain a vertical profile of the horizontal average intensity $\bar{I}(z, \Omega)$, i.e.,

$$\bar{I}(z, \Omega) = \left\langle \frac{1}{S} \int_S I_\gamma(x, y, z, \Omega) dx dy \right\rangle. \quad (1)$$

Here $\langle \cdot \rangle$ designates ensemble averaging, i.e., over all possible realizations of γ within a satellite pixel S . The mean intensity, $U(z, \Omega)$, incident on the leaf surface at depth z is another important statistical characteristics of the canopy radiation regime needed, for example, to estimate canopy energy absorption capacity. This variable is defined as

$$U(z, \Omega) = \frac{\left\langle \int_S I_\gamma(x, y, z, \Omega) \gamma(x, y, z) dx dy \right\rangle}{\left\langle \int_S \gamma(x, y, z) dx dy \right\rangle}. \quad (2)$$

It was shown (Shabanov et al., 2000; Titov, 1990; Vainikko, 1973) that under some reasonable physical assumptions of probabilistic properties of the indicator function, a small and simple system of deterministic 1D integral equations containing $\bar{I}(z, \Omega)$ and $U(z, \Omega)$ directly as its unknowns can be derived (Appendix A). The system requires two statistical characteristics of the 3D canopy structure as input. The first one characterizes the vertical heterogeneity of vegetation and is defined as the probability, $p(z)$, of finding a foliated point at depth z , i.e.,

$$p(z) = \left\langle \frac{1}{S} \int_S \gamma(x, y, z) dx dy \right\rangle. \quad (3)$$

The second parameter, a pair correlation function, describes correlation between foliated points and is defined as the probability,

$q(z, \xi, \Omega)$, of finding simultaneously foliated points on horizontal planes z and ξ along a given direction Ω , i.e.,

$$q(z, \xi, \Omega) = \left\langle \frac{1}{S} \int_S \gamma(r_z) \gamma(r_\xi - \ell \Omega) dx dy \right\rangle, \quad (4)$$

where $r_z=(x, y, z)$ is a point on the plane z , and ℓ is the distance between r_z and r_ξ (Fig. 2). If leaves are not spatially correlated with one another, then $q(z, \xi, \Omega)=p(z)p(\xi)$. The stochastic radiative transfer equations reduce to the conventional 1D radiative transfer equation in this case and $\bar{I}(z, \Omega)=U(z, \Omega)$ (Appendix B, Section 3).

The pair correlation function possesses a symmetry property in the form $q(z, \xi, \Omega)=q(\xi, z, -\Omega)$. This relationship directly follows from Eq. (4). Under some assumptions of the stochastic function $\gamma(r)$, the pair correlation function does not depend on the azimuth. In this case, it can be defined in terms of measures of the overlap between sets on a horizontal plane which, in turn, are functions of the horizontal distance (Chen et al., 1993; Strahler & Jupp, 1990; Jupp et al., 1988; also see Appendix C). It is convenient, therefore, to express arguments of the pair-correlation function in z, ξ and the horizontal distance λ (Fig. 2).

The structural parameters introduced above along with the leaf normal distribution function, the leaf scattering phase function and the leaf area volume density are required to specify the coefficients in the system of stochastic equations (Appendix A). We use the method of successive orders of scattering approximations (Shabanov et al., 2000) to numerically solve the system for $\bar{I}(z, \Omega)$ and $U(z, \Omega)$.

3. Monte Carlo models of the pair-correlation function

Consider a vegetation canopy consisting of identical trees resided in the layer $0 < z < H$. The tree crown is represented by a geometrical figure. In this section, non-dimensional scattering

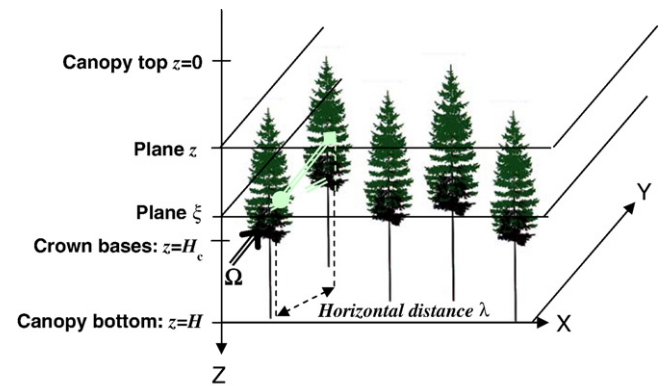


Fig. 2. Correlation between foliated points is described by the probability, $q(z, \xi, \Omega)$, of finding simultaneously foliated points on horizontal planes z and ξ along a direction Ω . Here two points $r_\xi=r_z-\ell \Omega$ (shown as a circle) and r_z (shown as a square) on the planes ξ and z ($z < \xi$) are spaced a distance ℓ apart along the upward direction Ω . The direction (unit vector) Ω has an azimuthal angle, ϕ , measured in the (XY) plane from the positive X axis in a counterclockwise fashion and a polar angle, θ , with respect to the polar axis that is opposite to the Z axis. The distance ℓ between r_z and r_ξ is given by $|z-\xi|/\cos \theta$. The horizontal distance, λ , is defined as horizontal projection of the line between r_z and r_ξ and given by $|z-\xi|\tan \theta$. For $z > \xi$ and downward directions, $q(z, \xi, \Omega)=q(\xi, z, -\Omega)$.

centres (leaves) are assumed to be uniformly distributed and spatially uncorrelated within tree crowns, i.e., the indicator function takes on the value 1 within tree crowns. Here we derive pair-correlations functions for cylindrical and conical in shape trees using a Monte-Carlo technique. A theoretical basis for deriving analytical equations for the pair correlation function in general case and further examples are given in Appendix C.

The following Monte Carlo procedure is implemented. A random number m of trees within a pixel area S is selected using the Poisson distribution $P(m) = (\bar{m})^m \exp(-\bar{m}) / m!$ where \bar{m} is the mean value of the random variable m . Random locations of m trees are generated with a uniform distribution function. If the running random location results in the intersection with previously simulated crowns, a tree is not positioned at this point and the next random location is generated. A realization of the canopy structure is the area S with m trees. Given z , ξ and Ω , one counts non-zero values of $\gamma(r_z)\gamma(r_z - \ell\Omega)$ for each realization of the canopy structure. Their ensemble average values are assigned to $q(z, \xi, \Omega)$.

Fig. 3 shows examples of Monte Carlo generated conditional correlation functions, $K(z, \xi, \Omega) = q(z, \xi, \Omega) / p(z)$, $z < \xi$, for cylindrical and conical in shape trees. They do not depend on the azimuth and are expressed in terms of z , ξ and the horizontal distance λ . There are several important features noteworthy in the correlation between two foliated points. First, for two points separated by a short horizontal distance, the values of $K(z, \xi, \lambda)$ are close to one. This is the effect of clumping of foliage elements; that is, detecting a leaf makes it more likely that the next leaf will be detected nearby. Note that Fig. 3 illustrates the effect of clumping of foliage into crowns while the curve “Cluster” in Fig. 4 accounts for both clumping of foliage into crowns and clumping of foliage within crowns. Second, a value

of the horizontal distance at which the correlation function reaches its minimum is related to the crown horizontal size at z . Third, with further increase in the horizontal distance, the correlation function tends to rise from its minimum to a constant value, and then levels off. This constant value is the probability, $p(\xi)$, of finding a foliated point at depth ξ . Beyond a distance at which the correlation function saturates, there is no relation between foliated points.

The derivative of the conditional pair-correlation function at the origin as λ tends to 0 is another important parameter which is diagnostic of the essential variability of canopy structure at the finest scale (Jupp et al., 1989; Roujean, 1999a). For example, for the Poisson germ-grain model (Appendix C, Section 1) of a forest consisting of identical cylindrical in shape trees, $|dK/d\lambda| = 4(1-g)\ln(1-g)/(\pi D_B)$ where g and D_B are ground cover and diameter of the crown base. If the derivative is near zero (e.g., the horizontal tree dimension D_B is large or the ground cover is close to 1), then vegetation canopy can be treated as a “smooth medium” whereas if it is high, then the canopy structure is “rough.” Inclusion of the within crown leaf spatial correlation will result in a finer scale of the canopy structure variability and values of $|dK/d\lambda|$ at $\lambda=0$ will consequently be increased (curve “Cluster” in Fig. 4).

For vertical directions, $\theta=0$ or $\theta=180^\circ$, the range of the horizontal distance reduces to a single point $\lambda=0$. The pair correlation function conveys information about mean vertical structure of the vegetation canopy. In Fig. 3, $K(z, \xi, 0) = 1$ if $z < \xi$ and thus $q(z, \xi, 0) = p(z)K(z, \xi, 0) = p(z)$. If $z > \xi$, $q(z, \xi, 0) = p(\xi)$ which is a direct consequence of the symmetry of the pair correlation function, i.e., $p(z)K(z, \xi, \lambda) = p(\xi)K(\xi, z, \lambda)$. In the limit $\xi \rightarrow z$, the function $K(z, z, \lambda)$ describes the horizontal distribution of phytoelements at z . In Fig. 3a, its values at distances between

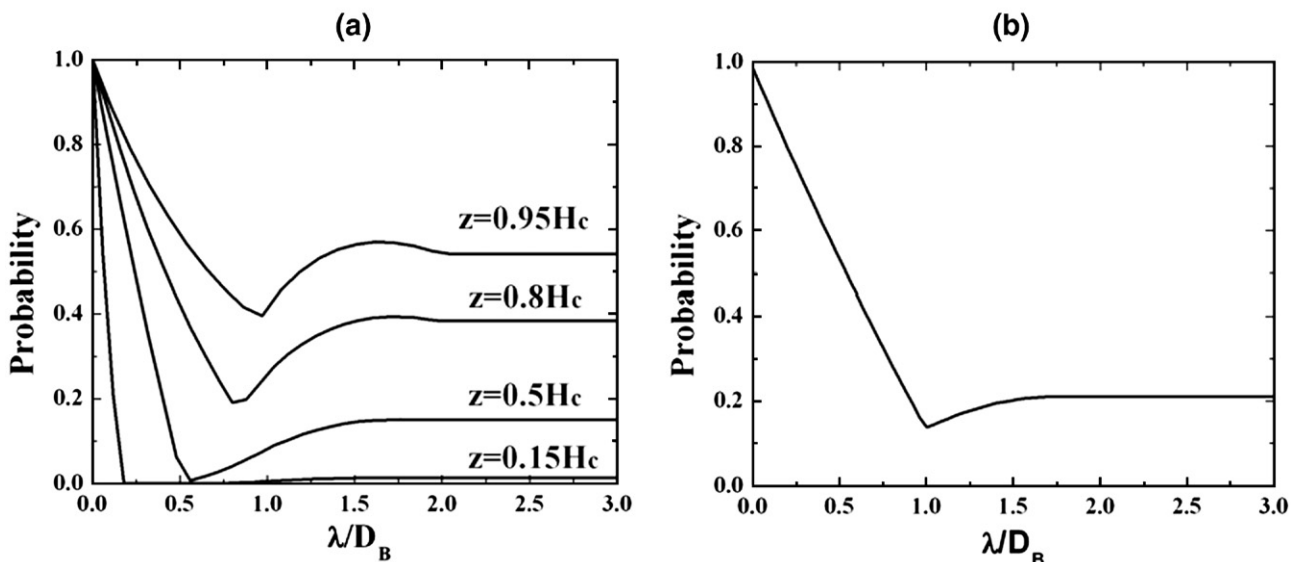


Fig. 3. Conditional probability, $K(z, \xi, \Omega) = q(z, \xi, \Omega) / p(z)$, of finding a foliated point at depth $\xi = z + \Delta z$ given that there is a leaf at depth z along the upward direction Ω for vegetation canopies consisting of conical (Panel a) and cylindrical (Panel b) in shape trees distributed in the canopy layer. Here $\Delta z = 0.01 \cdot H_c$ and H_c is the crown height. In these examples, the conditional pair correlation functions are independent of the azimuth and are expressed in z , ξ and the horizontal distance λ (Fig. 2). The dimensionless horizontal axis shows values of λ/D_B where D_B is the diameter of the crone base. If the horizontal dimension of tree crown varies with the depth, the conditional pair correlation function depends on z , ξ and λ (left panel). Otherwise, its values are determined by the horizontal distance λ only (right panel, see also Appendix C).

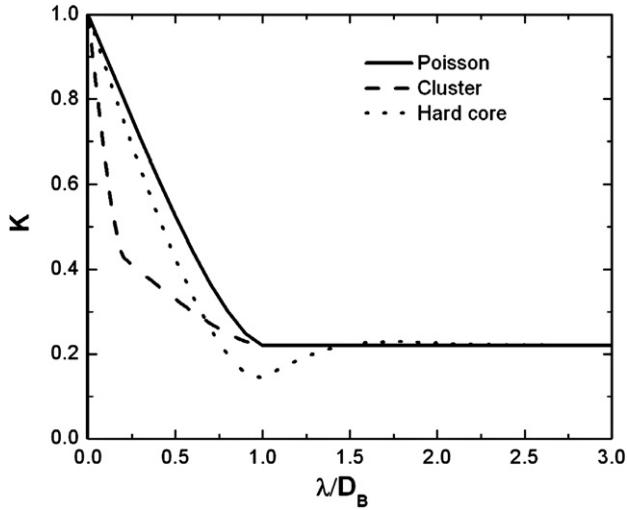


Fig. 4. Conditional pair correlation functions of the Poisson germ-grain, Matérn cluster and Matérn hard-core processes (Appendix C). Cluster, D_0 , and clump, D_c , sizes in the Matérn cluster process are set to D_B and $0.2D_B$, respectively. The probability, $p(z)$, of finding a foliated point at depth z is 0.22 in all examples.

tree diameter $D(z)$ at depth z and about $2D(z)$ are mainly determined by the probability of finding two trees placed λ apart. In between these extremes, the pair correlation function describes variation in the canopy structure along different directions, e.g., the distribution of phytoelements that shade leaves at depth ξ along a given direction Ω . To summarize, the pair-correlation function provides a quantitative description of the canopy structure and effects of all scales.

4. Three-dimensional effects of canopy structure on canopy radiation regime

The pair correlation function naturally arises from ensemble averaging the 3D canopy radiation field (Shabanov et al., 2000) and, therefore, determines its mean characteristics. The aim of this section is to illustrate that the foliage spatial correlation is primary responsible for the effects of the 3D canopy structure on canopy reflective and absorptive properties.

The Poisson germ-grain model of the forest with equal cylindrical in shape trees (Appendix C, Section 1) is used to simulate the 3D canopy structure. The crown height coincides with the canopy depth H , i.e., the canopy layer $0 < z < H$ consists of tree crowns. The diameter of the crown base is D_B . Non-dimensional scattering centres (leaves) are assumed to be uniformly distributed and spatially uncorrelated within tree crowns. The probability, $p(z)$, of finding a foliated point at depth z (Eq. (3)) is constant in this case and coincides with the ground cover g , i.e., $p(z) = g$. The pair correlation function is given by Eq. (C3a). The amount of leaf area in the tree crown is parameterized in terms of the plant LAI defined as $L_0 = d_L H$. The canopy LAI is gL_0 .

A uniform and bi-Lambertian models are assumed for the leaf normal distribution and the diffuse leaf scattering phase function, respectively (Ross, 1981). Leaf hemispherical reflectance and transmittance are assumed to have the same value and set to 0.07 at the red and 0.38 at the near-infrared wavelength.

Soil reflectance is variable in our calculations. The vegetation canopy is illuminated by a parallel beam of unit intensity. The solar zenith angle and azimuth of the incident radiation are set to 30° and 0° , respectively.

Our calculations include two steps. First, we solve the stochastic transport equations for mean intensities $\bar{I}(z, \Omega)$ and $U(z, \Omega)$. Second, we average the 3D canopy structure into a 1D medium first and then solve the stochastic radiative transfer equation. For the 1D medium, the ground cover is one and values of the plant and canopy LAIs coincide (i.e., $L_0 = \text{LAI}$). The pair correlation function is independent of z , ξ and λ , and equal to unity, i.e., the leaves become uncorrelated. The mean intensity $\bar{I}(z, \Omega)$ coincides with the solution of the conventional 1D radiative transfer equation and $U(z, \Omega) = \bar{I}(z, \Omega)$ (Appendix B, Section 3). The difference in the mean intensities of the 3D and 1D vegetation canopies will be used as a measure to quantify the effect of canopy structure on the canopy radiation regime.

An alternative way to construct a 1D canopy structure is to ignore the leaf spatial correlation by setting the conditional pair correlation function to its saturated value, i.e., $K(z, \xi, \Omega) = g$ (Fig. 4, curve ‘‘Poisson’’). Formally, the canopy structure is parameterized in terms of the ground cover and the plant leaf area index in this case. The solutions of the stochastic transport equations, however, depend on the product gL_0 but not on absolute values of g and L_0 if the pair correlation function does not vary (Appendix B, Section 4). The two methods, therefore, result in the same mean intensities.

4.1. Vertical profiles of radiation fluxes

Here we investigate the effects of the 3D canopy structure on canopy radiation regime by comparing the first and second moments of vertical profiles of the radiation flux densities. The former represents an average of the within and between crown radiation fields while the latter is the mean radiation regime within a tree crown. Definitions of the up- and downward radiation flux densities are given in Appendix B.

Fig. 5 presents vertical profiles of mean downward and upward radiation flux densities accumulated over crown horizontal cross sections (F_U^\downarrow and F_U^\uparrow), and over the horizontal plane (F_I^\downarrow and F_I^\uparrow). Their differences, $F_I^\downarrow(z) - F_U^\downarrow(z)$, at red and near-infrared wavelengths for $g=0.5$ and 1 are shown in Fig. 6. It follows from Eq. (B4) that

$$F_I^\downarrow(z) - F_U^\downarrow(z) = (1 - g)[F_U^\downarrow(z) - F_U^\uparrow(z)]. \quad (5)$$

Here $F_U^\downarrow(z)$ denotes the mean downward (upward) radiation flux density accumulated over gaps at depth z (Appendix B).

The 1D vegetation canopy (solid lines in Figs. 5 and 6) does not discriminate between tree crowns and gaps between them and thus $F_U^\downarrow(z) = F_U^\uparrow(z) = F_I^\downarrow(z) = F_I^\uparrow(z)$. In this example, the conditional pair correlation function accounts for the clustering of foliage into tree crowns. It reaches its maximum value of 1 at $\lambda=0$ (Fig. 3) indicating that there are more scattering centers and, consequently, more foliage–radiation interactions at small scales than the 1D approach assumes. Attenuation of the flux densities by the foliage is stronger than the 1D approach predicts (Fig. 5),

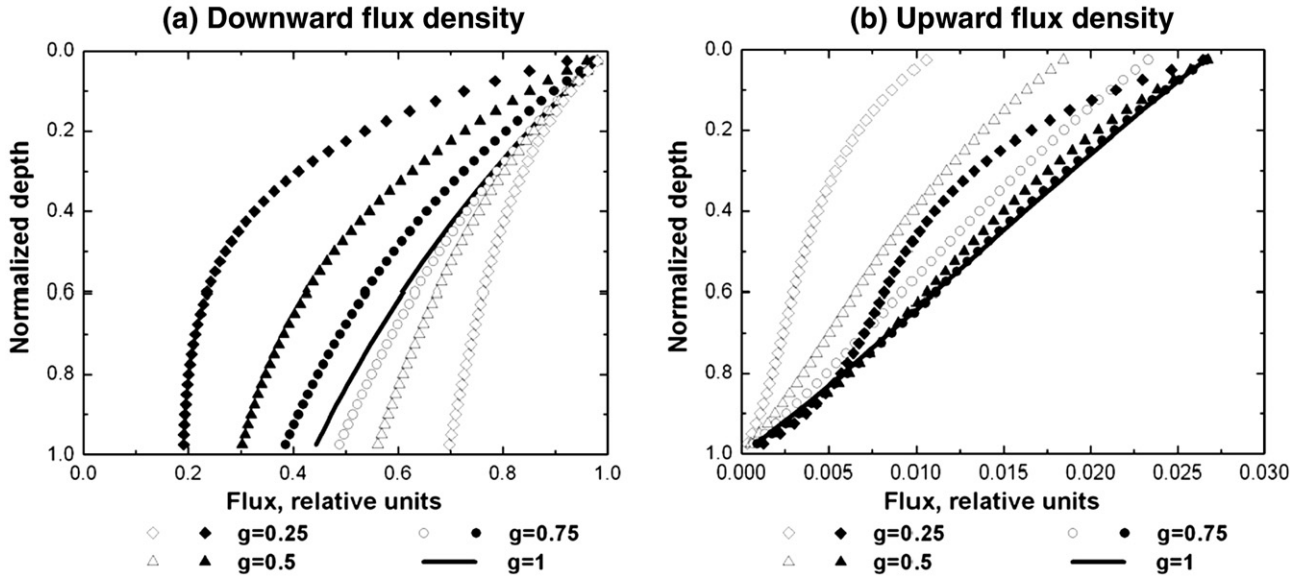


Fig. 5. Vertical profiles of mean downward (Panel a) upward (Panel b) radiation flux densities at red wavelength for four values of the ground cover g . Ground reflectance is zero. Canopy LAI is fixed and set to 1.5. Plant LAI varies with the ground cover as $1.5/g$. The case $g=1$ (solid lines) corresponds to the 1D vegetation canopy. Solid and hollow symbols represent mean flux densities over crown horizontal cross sections and over the entire horizontal plane, respectively. The dimensionless horizontal axis shows values of z/H_c where H_c is the crown height.

i.e., $F_{\downarrow}^{\uparrow}(z) \leq F_{\downarrow}^{\downarrow}(z)$. In this example, $LAI = gL_0$, a decrease in the ground cover g enhances the within crown photon interactions due to an increase in the plant leaf area index L_0 (Fig. 5).

Tree crowns transmit less radiation compared to horizontally averaged values, i.e., $F_{\downarrow}^{\uparrow}(z) < F_{\downarrow}^{\downarrow}(z)$ (Fig. 5a). It follows from this inequality and Eq. (5) that $F_{\downarrow}^{\uparrow}(z) > F_{\downarrow}^{\downarrow}(z)$ and thus gaps between trees are primarily responsible for the propagation of radiant energy in downward directions. In contrast, upward fluxes have the opposite tendency, i.e., $F_{\downarrow}^{\uparrow}(z) > F_{\downarrow}^{\downarrow}(z)$ (Fig. 5b). For a vegetation canopy bounded from below by a non-reflecting surface, the scattering from leaves determines the upward radiation field. With a fixed amount of the total leaf area, the

upward radiation field is an increasing function with respect to the ground cover since an increase in the ground cover involves a decrease in gaps between trees which do not “participate” in the scattering process. As one can see from Fig. 6, these tendencies also take place at near-infrared wavelength.

The reflection, $F_{\downarrow}^{\uparrow}(0)$, of tree crowns is close to the reflection, $F_{\downarrow}^{\downarrow}(0)$, of the 1D canopy. The mean canopy reflection results from both scattering occurred in tree crowns and “zero scattering” in the between crown space. This lowers the mean canopy reflectance. The 1D approach ignores the gap effect and mean upward radiation flux densities are consequently overestimated.

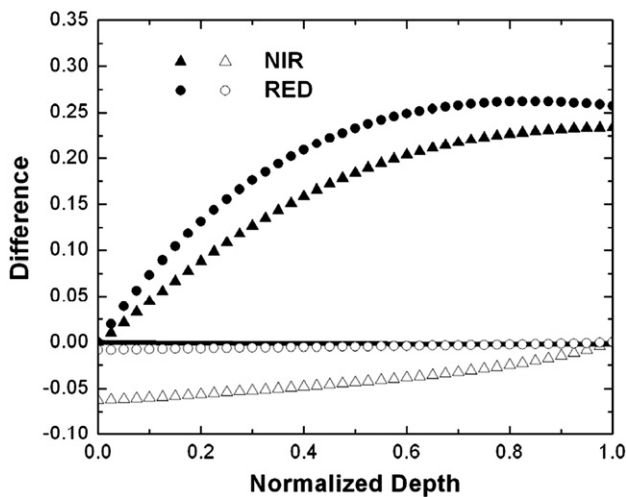


Fig. 6. Difference between mean downward (upward) flux densities over the horizontal plane and over crown horizontal cross sections at red and near-infrared wavelengths. Solid line represents 1D vegetation canopy ($g=1$) while symbols corresponds to $g=0.5$. Solid and hollow symbols show the difference in downward and upward flux densities, respectively. Other parameters are as in Fig. 5.

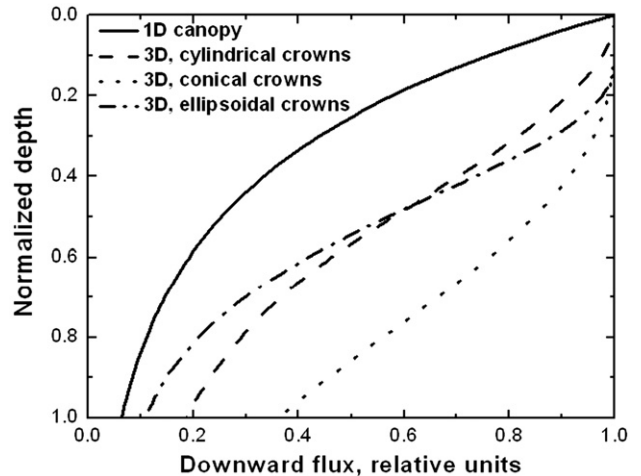


Fig. 7. Vertical profiles of mean downward radiation flux densities over between crown space at red wavelength. Calculations are performed for vegetation canopies consisting of cylindrical (dashed line), conical (dotted line) and ellipsoidal (dashed-dotted line) in shape trees. A 1D vegetation canopy is also shown for comparison (solid line). Canopy LAI and ground cover are 4.2 and 0.85, respectively. Soil reflectance is zero.

The sigmoidal shapes of the vertical distribution of the between crown downward fluxes have been reported in several studies (Larsen & Kersaw, 1996; Ni et al., 1997; Roujean, 1999a,b). The clumping of phytoelements into tree crown is primarily responsible for this 3D effect (Roujean, 1999b). Fig. 7 shows mean vertical profiles of downward fluxes, $F_{\downarrow}^{\downarrow}(z)$, averaged over the between crown space. Calculations are performed for vegetation canopies consisting of cylindrical, conical and ellipsoidal in shape trees. Eqs. (C2a)–(C2d) are used to specify corresponding pair-correlation functions and probabilities, $p(z)$, of finding a foliated point at depth z . In these examples, the ground cover, $g = \max p(z)$, and canopy leaf area index, $LAI = d_L \int_0^H p(z) dz$, are fixed and equal to 0.85 and 4.2, respectively. Maximum radii of the crown horizontal cross-sections are set to $0.25H$ where the crown (canopy) height H is 1 (in relative units). One can see that the vertical profiles follow the sigmoidal distribution and are sensitive to the crown shape. The simulated distributions conform to both theoretical and empirical expectations (Ni et al., 1997; Roujean, 1999b).

To summarize, the 1D canopy model which admits only the amount of leaf area and not its spatial distribution, does not discriminate between the radiative regimes within and between crowns. This results in underestimation of the mean downward horizontal fluxes and overestimation of its upward counterpart. The discrepancy is especially greater at lower ground covers. Ignoring within and between crown radiation regimes can lead to incorrect predictions of solar fluxes in the forest canopy. Note that the effects captured by the stochastic radiative transfer equation are consistent with three-dimensional effects reported in literature (Asrar et al., 1992; Ni et al., 1997; Roujean, 1999a,b).

4.2. Energy conservation law

Many ecosystem productivity models and global models of climate, hydrology and ecology need an accurate information on how solar energy is distributed between vegetation canopies and

the ground. Using the NCAR Community Climate Model, Buermann et al. (2001) reported that a more realistic partitioning of the incoming solar radiation between the canopy and the underlying ground results in improved model predictions of near-surface climate. The vegetation structure determines the partitioning of the incoming radiation between canopy absorption, transmission and reflection. This section shows examples of 3D effects of canopy structure on the shortwave energy balance.

Fig. 8 shows mean canopy reflectance, $F_{\uparrow}^{\uparrow}(0)$, and transmittance, $F_{\uparrow}^{\uparrow}(1)$. For a vegetation canopy bounded from below by a non reflecting surface, the canopy absorptance is $1 - F_{\uparrow}^{\uparrow}(0) - F_{\uparrow}^{\uparrow}(1)$. The 1D approach underestimates canopy transmittance and overestimates canopy reflectance at both red and near infrared wavelengths. As one can see from Fig. 9, these two opposite tendencies do not compensate each other, resulting in an overestimation of canopy absorptance.

The results given in Fig. 9 show that at a given canopy LAI, canopy absorptance can differ depending upon ground cover and plant LAI. This is not a surprising result because a given amount of leaf area can be distributed in different ways in a canopy, for instance, as canopies of dense trees (high plant LAI) with low ground cover or as canopies of sparse trees (low plant LAI) with high ground cover. Although the canopy LAI is the same in both cases, the between and within crown radiation regimes are different. Gaps between trees enhance the canopy transmittance at the expense of the canopy absorptance and reflectance. An increase in ground cover involves a decrease in gaps between tree crowns which contribute neither to canopy absorptance nor canopy reflectance. This process enhances canopy reflective (Fig. 8) and absorptive (Fig. 9) properties. It should also be noted that variation in canopy reflectance, absorptance and transmittance with the canopy LAI happens at a lower rate than the 1D predicts (Figs. 8 and 9). Ignoring the within and between crown radiation regimes can lead to overestimation of the saturation domain, i.e., a range of canopy reflectance values which are insensitive to variation in canopy structure (Fig. 1).

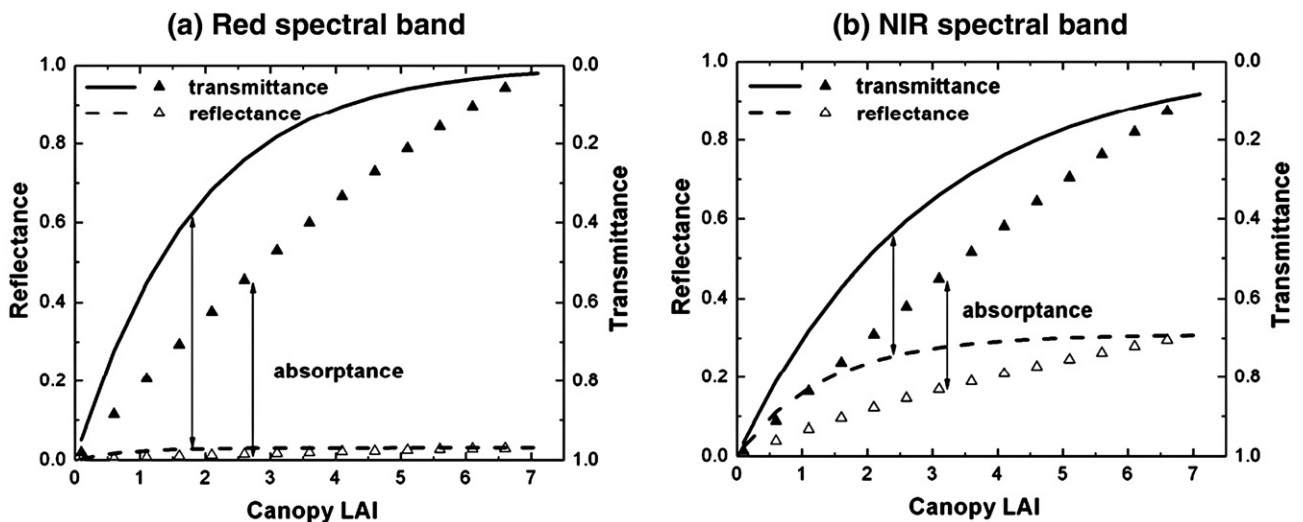


Fig. 8. Mean canopy reflectance $F_{\uparrow}^{\uparrow}(0)$ (vertical axis on the left side) and transmittance $F_{\uparrow}^{\uparrow}(1)$ (vertical axis on the right side) at red (Panel a) and near-infrared (Panel b) wavelengths as a function of the canopy LAI. Solid and dashed lines represent the 1D canopy while symbols show its 3D counterpart. Ground reflectance is zero. The canopy absorptance is $1 - F_{\uparrow}^{\uparrow}(0) - F_{\uparrow}^{\uparrow}(1)$ (arrows). Plant leaf area index L_0 is fixed and set to 7. Ground cover varies with the canopy LAI as $g = LAI/L_0 = LAI/7$.

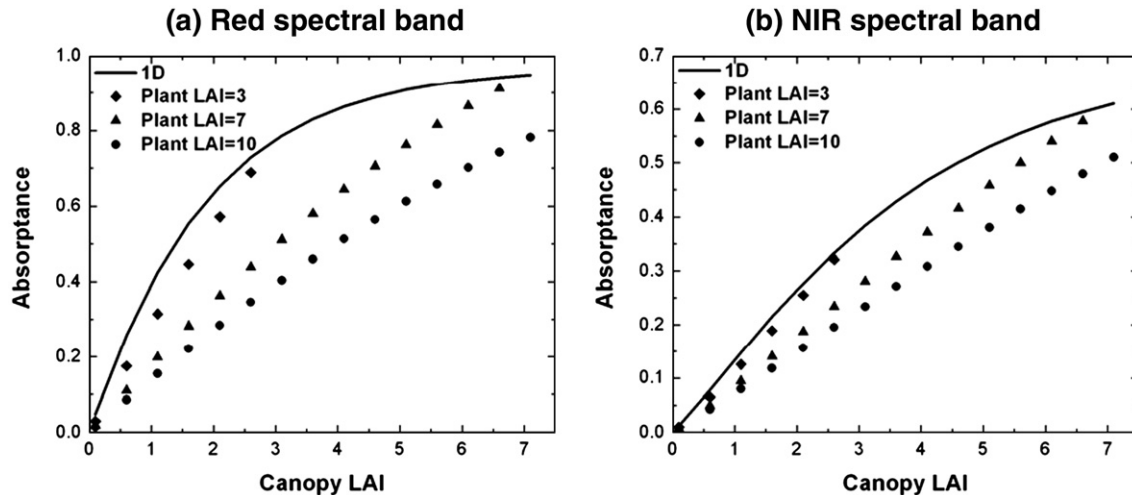


Fig. 9. Mean canopy absorbance at red (Panel a) and near infrared (Panel b) wavelengths as a function of canopy LAI for three values of the plant leaf area index L_0 . Solid line and symbols represent 1D and 3D vegetation canopies, respectively. Ground cover, g , varies with the canopy LAI as $g=LAI/L_0$. Other parameters are as in Fig. 8.

The spatial distribution of trees significantly affects the between and within crown radiation regimes which, in turn, determine the short wave energy conservation law in vegetation canopies. The stochastic radiative transfer equations provide vertical profiles of the horizontal mean, $\bar{I}(z, \Omega)$, and the second moment, $U(z, \Omega)$, of the 3D radiation field and thus is able to discriminate between radiative regimes occurred in crowns and in a space between them. The impact of 3D canopy structure on the partitioning of incoming radiation between canopy transmittance, reflectance and absorbance, therefore, is captured by the stochastic radiative transfer equations.

4.3. Geometric effect

A vegetated surface scatters shortwave radiation into an angular reflectance pattern, or Bidirectional Reflectance Factor (BRF), whose magnitude and shape are governed by the composition, density, optical properties and geometric structure of the vegetation canopy and its underlying surface. By definition, the BRF is the surface leaving radiance divided by radiance from a Lambertian reflector illuminated from a single direction (Martonchik et al., 2000). Satellite-borne sensors measure the mean radiation field emanating from a satellite pixel, i.e.,

$$\text{BRF}(\Omega, \Omega_0) = \frac{\bar{I}(0, \Omega)}{\pi^{-1} \mu_0 i_0}. \quad (6)$$

Note that this parameter has been operationally produced from data provided by the MODIS and MISR instruments during the Earth Observing System (EOS) Terra mission (Bothwell et al., 2002; Schaaf et al., 2002).

Fig. 10 shows the BRF at red wavelength in the nadir view direction for a vegetation canopy bounded from below by a reflecting surface. For sparse vegetation canopies, photons reflected from the sunlit area of the underlying surface can escape the 3D canopy in the nadir direction without experiencing a collision. This 3D effect results in increased canopy brightness at low ground cover. The BRF exhibits a non monotonic variation

with the ground cover. First, it decreases since an increase in the ground cover involves a decrease in the sunlit area which, in turn, reduces the impact of the between crown radiation on the BRF in the nadir direction. Second, at sufficiently large ground cover values, the contribution of the underlying surface vanishes and, as in the case of a vegetation canopy with a non-reflecting surface (Figs. 5b and 8), the BRF becomes an increasing function with respect to the ground cover. As discussed earlier, the 3D effects make its values lower compared to those evaluated with the 1D model. If the leaf spatial correlation is ignored, i.e., $q(z, \xi, \Omega) = g^2$, the BRF becomes independent of the ground cover. Thus ignoring the leaf spatial correlation can result in an underestimation of the contribution of canopy background to the canopy leaving radiation for sparse and intermediately dense vegetations and an overestimation of the canopy BRF for dense vegetations.

The importance of accounting for 3D effects in algorithms for the estimating of leaf area index from satellite data is illustrated in Fig. 11. In this example, LAI values over evergreen needle

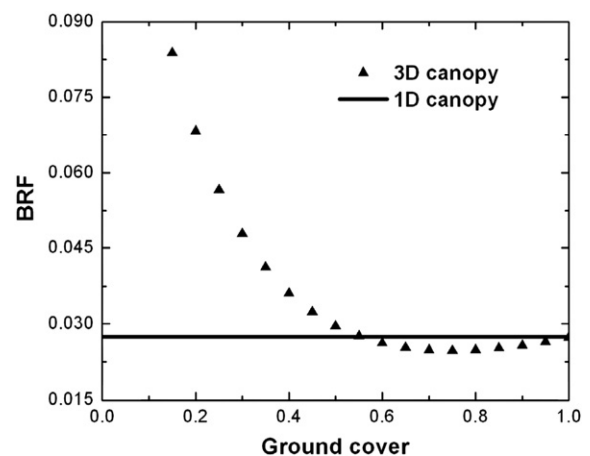


Fig. 10. Bidirectional Reflectance Factor (BRF) at red wavelength in nadir view direction as a function of ground cover. Solid line and symbols represent 1D and 3D vegetation canopies, respectively. Canopy LAI is fixed and set to 7. Plant leaf area index varies with ground cover, g , as $7/g$. Surface albedo is 0.18. The solar zenith angle is 30° . Other parameters are as in Fig. 8.

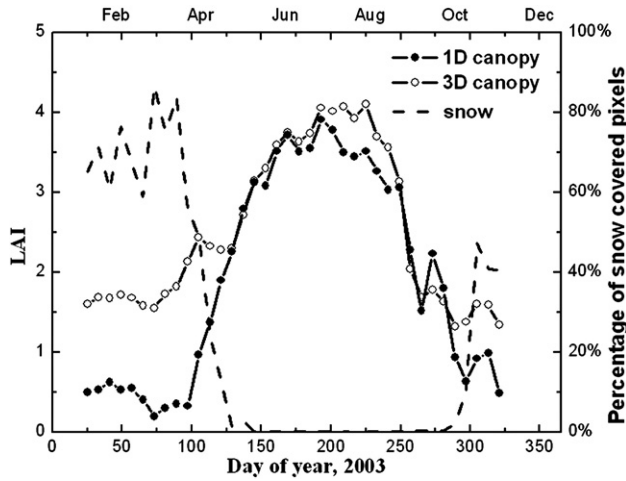


Fig. 11. Annual course of the mean LAI (vertical axis on the left side) over evergreen needle leaf forests located in an area of 1200 km by 1200 km (the MODIS tile h12v03) derived from MODIS data using the MODIS LAI&FPAR operational algorithm with look-up-tables generated by the stochastic RTE that accounts for the foliage spatial correlation (legend “3D canopy”) and ignores it (legend “1D canopy”). Also shown is the annual course of the percentage of snow covered pixels in the MODIS tile (dashed line, vertical axis on the right side).

leaf forest at 1 km resolution are derived from the MODIS atmosphere corrected surface reflectance product (Justice et al., 2002) using the MODIS LAI&FPAR operational algorithm (Knyazikhin et al., 1998b) which performs retrievals by comparing observed spectral BRFs to comparable values from model-based canopy reflectances stored in a look-up-table. The algorithm was run two times per pixel, each time with a different look-up-table. In the first case, the BRFs for a suite of canopy structures, ground reflectances and sun-view geometries that represents an expected range of typical conditions were calculated using the stochastic radiative transfer equation and the Poisson germ-grain model of the forest with equal cylindrical in shape trees (Appendix C, Section 1). In the second case, the

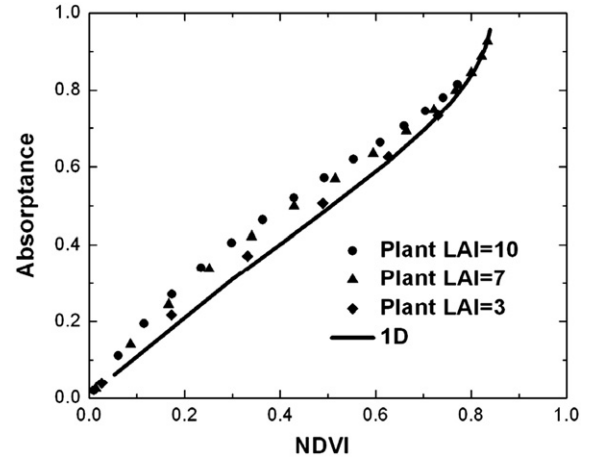


Fig. 13. Canopy absorption at red wavelength versus Normalized Difference Vegetation Index (NDVI). All parameters are set to the same values as in Fig. 12.

look-up-table was generated without accounting for the leaf spatial correlation, i.e., the pair-correlation function $q(z, \xi, \Omega)$ was set to g^2 . The use of the 1D canopy structure in the retrieval technique results in substantial underestimation of the contribution of high reflecting snowy background to the canopy BRF and the portion of radiation reflected by trees is consequently overestimated. This causes unrealistically low values of winter time LAIs over evergreen needle leaf forests. This example suggests that ignoring 3D effects in the 1D models of the canopy structure can lead to incorrect estimation of the vegetation seasonality.

4.4. Canopy structure and NDVI

The measured spectral reflectance data are often transformed into vegetation indices. More than a dozen such indices are reported in the literature and shown to correlate well with vegetation amount (Tucker, 1979), the fraction of absorbed photosynthetically active radiation (FPAR) (Asrar et al., 1984),

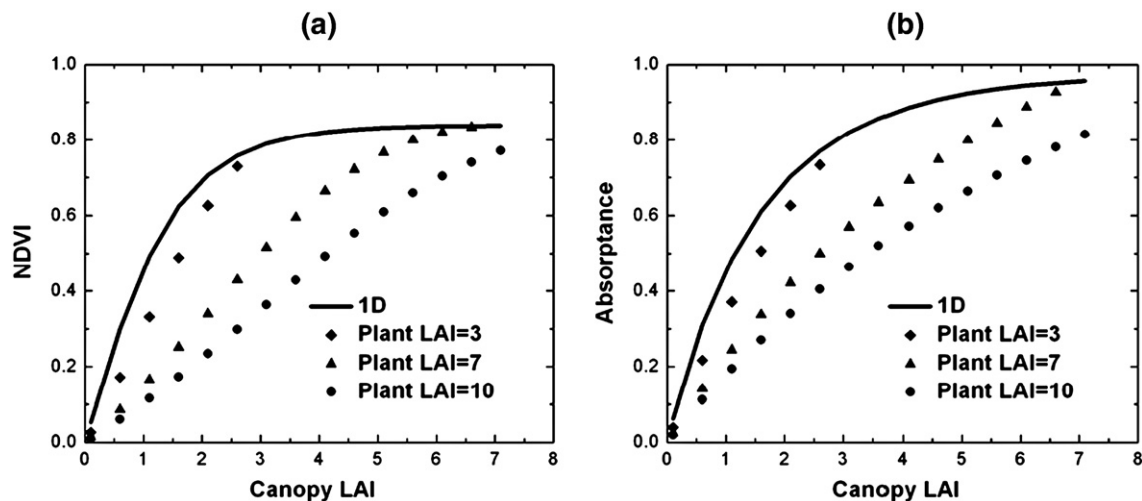


Fig. 12. Normalized Difference Vegetation Index (Panel a) and canopy absorption at red wavelength (Panel b) versus canopy LAI for three values of plant leaf area index L_0 . Solid line and symbols represent 1D and 3D vegetation canopies, respectively. Ground cover varies with the canopy LAI as $g=LAI/L_0$. Surface albedo is 0.18 at red and near infrared wavelengths. Other parameters are as in Fig. 9.

Table 1
Characteristics of the SSA Old Jack Pine (SSAOJP) and SSA Old Aspen (SSAOA) sites used for model parameterization

Site	Age, years	Stem density, stems/ha	LAI	Understory LAI	Tree height, m	Crown length, m	Horizontal Crown radius, m	Leaf/needle reflectance		Leaf/needle transmittance		Understory reflectance	
								RED	NIR	RED	NIR	RED	NIR
SSAOJP	68	2700	2.2	0	12.7	7	1.2	0.10	0.62	0.028	0.31	0.15	0.29
SSAOA	60	1200	2.3	3.23	16.2	10.76	2.12	0.065	0.36	0.135	0.60	0.09	0.40

unstressed vegetation conductance and photosynthetic capacity (Sellers et al., 1992), and seasonal atmospheric carbon dioxide variations (Tucker et al., 1986). This section shows examples of 3D effects of canopy structure on relationships between canopy absorption, LAI and the normalized difference vegetation index.

The normalized difference vegetation index, NDVI, is defined as the ratio between the difference and the sum of bidirectional reflectance factors at near infrared, BRF_{NIR} , and red, BRF_{RED} , wavelengths, i.e.,

$$NDVI(\Omega, \Omega_0) = \frac{BRF_{NIR}(\Omega, \Omega_0) - BRF_{RED}(\Omega, \Omega_0)}{BRF_{NIR}(\Omega, \Omega_0) + BRF_{RED}(\Omega, \Omega_0)}. \quad (7)$$

Note that this parameter has been operationally produced from data provided by the MODIS instrument during the Earth Observing System (EOS) Terra mission (Huete et al., 2002). Here we consider the NDVI at the nadir view direction.

The relationships between canopy absorptance and NDVI versus canopy LAI are shown in Fig. 12. The results are similar to those shown in Fig. 9, i.e., at a given canopy LAI, canopy absorptance and NDVI can differ depending upon ground cover and plant LAI. Different radiation regimes in tree crowns and gaps between them are primarily responsible for this effect. Values of canopy absorptance versus corresponding NDVI values are plotted in Fig. 13. One can see that the impact of 3D

canopy structure on the absorptance–NDVI relationship is minimal. This effect is consistent with the results documented in Asrar et al. (1992), i.e., spatial heterogeneity in vegetation canopies does not affect the relationship between NDVI and fraction of absorbed photosynthetically active radiation (FPAR). The relationship is also insensitive to rather large changes in solar zenith angle (Asrar et al., 1992; Kaufmann et al., 2000). It should be noted, however, that the NDVI–FPAR relationship is sensitive to the background. Theoretical analyses of these regularities are established in (Kaufmann et al., 2000; Knyazikhin et al., 1998b; Myneni et al., 1995).

5. Evaluation of the stochastic approach

The BRF measurements made with the PARABOLA (Deering & Leone, 1986) on two boreal forest study sites during field campaigns in central Saskatchewan, Canada, in 1994 (Deering et al., 1999) are used to validate the stochastic radiative transfer equations. The sites representative of coniferous and broadleaf forests are located in the Southern Study Area (SSA) of the Boreal Ecosystem–Atmosphere Study (BOREAS) experiment. The BOREAS designated names for these sites are SSA Old Jack Pine (OJP, 53.916°N, 104.69°W) and SSA Old Aspen (OA, 53.63°N, 106.20°W). These sites were the subject of intensive field campaigns carried out in 1994 as part of BOREAS field activities. A field data set includes forest age, stem density, overstory and understory LAIs (Deering

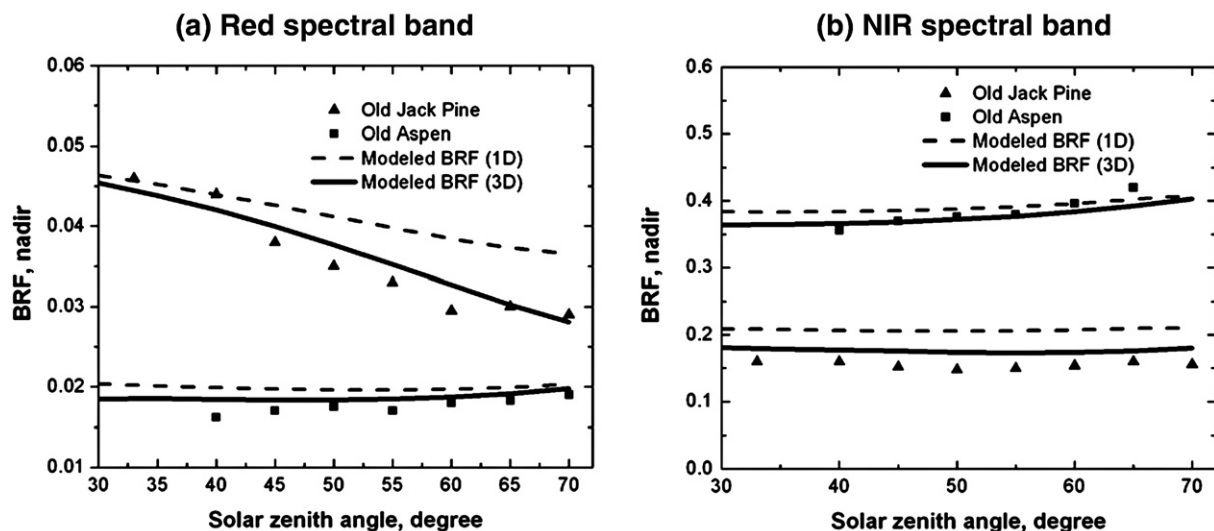


Fig. 14. Bidirectional Reflectance Factor at red (Panel a) and NIR (Panel b) wavelengths in the nadir direction as a function of the solar zenith angle for the SSAOJP and SSAOA sites. Symbols represent measured BRFs. Solid and dashed lines show simulated BRF using 3D and 1D models of canopy structure, respectively.

Table 2

Root mean square error in predicted nadir bidirectional reflectance factor at red (650–670 nm) and near infrared (810–840 nm) spectral bands for the SSA Old Jack Pine (SSAOJP) and SSA Old Aspen (SSAOA) sites

	Red spectral band		NIR spectral band	
	SSAOJP	SSAOA	SSAOJP	SSAOA
3D canopy	0.0021	0.0013	0.021	0.013
1D canopy	0.0061	0.0024	0.053	0.016

et al., 1999), tree height, crown height and horizontal crown radius (Chen, 1996; Hardy et al., 1998), optical properties of leaves, needles and understory (Middleton & Sullivan, 2000; Miller et al., 1997). The characteristics of each site are summarized in Table 1. Their detailed description can be found in Deering et al. (1999).

The PARABOLA instrument permits acquisition of radiance data in three narrow spectral bands (650–670 nm, 810–840 nm, and 1620–1690 nm) for almost the complete (4π) sky-and ground-looking hemispheres in 15° instantaneous field of view (IFOV) sectors in 11 s (Deering et al., 1999). The following sampling strategy was employed to measure the forest canopy BRF at the SSAOJP and SSAOA sites (Deering et al., 1999). The PARABOLA instrument was suspended from a tram which traversed a pair of fixed steel cables between two towers spaced about 70 m apart. The tram cable height was about 13–14 m above the canopy height at each site. This sampling height and the instrument IFOV of 15° resulted in a nadir view footprint size at canopy top level of about 9 m^2 , increasing to about 79 m^2 at 60° off-nadir view angle (Deering et al., 1999). PARABOLA measurements were taken at distances from 25 m to 5 m from a tower, at 2 m increments. This resulted in a total 11 measurements being taken along the tram at each solar zenith angle. The data were processed to obtain mean BRF over sampling points in 15° angular increments in view zenith angle and 30° angular

increments of view azimuth with one of the bins being centered on the solar principal plane (Deering et al., 1999).

The Poisson germ-grain model of the forest with identical cylindrical trees (Appendix C, Section 1) is used to simulate canopy structure of the SSAOJP and SSAOA sites. The ground cover is estimated with Eq. (C2b) where the stem density d and the crown radius $r(z)=D_B/2$ are given in Table 1. Its value is 0.71 for the SSAOJP and 0.82 for the SSAOA site. Given ground cover, the pair-correlation function was calculated using Eq. (C3a). The plant leaf area index, $L_0=LAI/g$, and the leaf area volume density, $d_L=L_0/H_c$ are $L_0=3.12$, $d_L=0.46$ for SSAOJP and $L_0=2.82$, $d_L=0.26$ for SSAOA. Here H_c and LAI are the crown height and the canopy LAI (Table 1).

The radiative transfer equation requires specification of the scattering and extinction coefficients at a scale of the mean photon free path (mean distance of photon travel between two consecutive interactions). In coniferous canopies, clumped shoot structure causes multiple scattering within a shoot, i.e., at a needle and finer scales. The coefficients can not be specified because fluctuations of the number of needle in a given volume do not follow Poisson statistics at these scales (Chen & Leblanc, 1997; Nilson, 1999). In radiative transfer models for conifers, therefore, a shoot is usually taken as the basic structural element (Rautiainen & Stenberg, 2005; Smolander & Stenberg, 2003, 2005; Stenberg, 1996). The shoot scattering coefficient, ω_{sh} , is calculated based on the canopy spectral invariant applied to the shoot (Huang et al., 2007; Smolander & Stenberg, 2003)

$$\omega_{sh} = \omega_n \frac{1 - p_{sh}}{1 - p_{sh}\omega_n} \quad (8)$$

Here ω_n is the needle albedo (needle reflectance plus needle transmittance, Table 1) and p_{sh} is the probability that a photon scattered from a needle in the shoot will interact within the same shoot again — the shoot recollision probability. The latter is related to the spherically averaged shoot silhouette to total needle

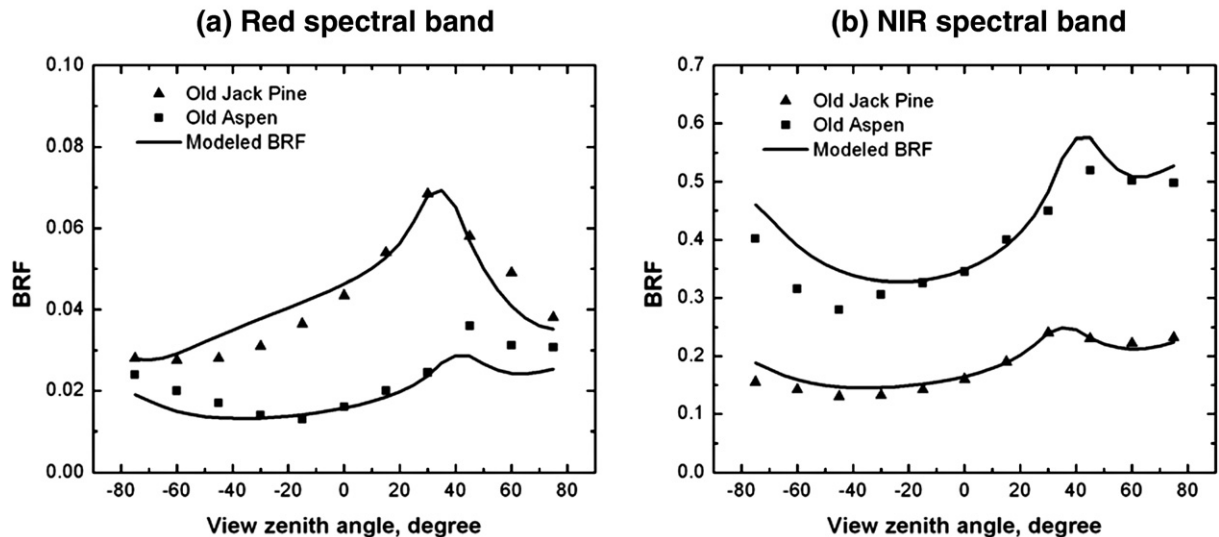


Fig. 15. Bidirectional Reflectance Factor in the solar principal plane at red (Panel a) and NIR (Panel b) wavelengths for the SSAOJP and SSAOA sites. The solar zenith angles are 34° for SSAOJP and 40° for SSAOA. Solid line and symbols represent predicted values and PARABOLA measurements. The RMSE values at red and near infrared spectral bands are 0.0042 and 0.014 for the SSAOJP, 0.0043 and 0.042 for the SSAOA sites.

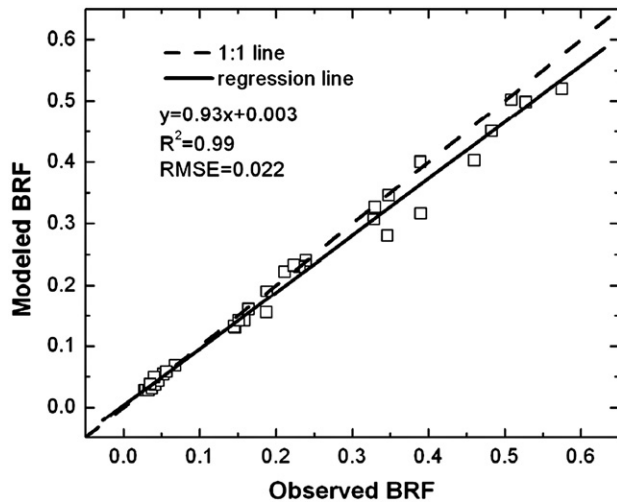


Fig. 16. Correlation between measured and simulated Bidirectional Reflectance Factors in the solar principal plane at red and NIR wavelengths for the SSAOJP and SSAOA sites. The solar zenith angles are 34° for SSAOJP and 40° for SSAOA. The view zenith angle varies from 0° to 70° in 15° angular increments. The R^2 and RMSE are 0.99 and 0.0022, respectively. The measured and modeled values follow the regression line $y=0.93x+0.003$.

area ratio, $\overline{\text{STAR}}$, as $P_{\text{sh}} = 1 - 4\overline{\text{STAR}}$ (Smolander & Stenberg, 2003). The radiative transfer equation can now be applied to describe shoot-photon interaction. The within-shoot multiple scattering is accounted by the shoot recollision probability appeared in the scattering coefficient (Smolander & Stenberg, 2005). The value of p_{sh} was set to 0.44 corresponding to an average value of $\overline{\text{STAR}} = 0.14$ (Oker-Blom & Smolander, 1988).

Measured and modeled BRFs at red and NIR wavelengths in the nadir direction as a function of the solar zenith angle for the SSAOJP and SSAOA sites are shown in Fig. 14. The BRFs simulated using the 3D model of canopy structure show very good agreement with measurements (Table 2). If one simplifies the canopy structure into a 1D medium by setting the conditional pair correlation function to its saturated value, ground cover g , the disagreement increases by a factor of about 2.7 for the SSAOJP and 1.5 for SSAOA site (Table 2). In both cases, the 1D approach overestimates the observations. This result is consistent with simulations shown in Fig. 14. The effect of ignoring the leaf spatial correlation is more pronounced at lower ground covers, as expected.

A statistical model proposed by Shabanov et al. (2000) is used to simulate the hot spot effect (a sharp peak in reflected radiation about the retro-solar direction). The model requires the specification of a coefficient related to the ratio of vegetation height to the smallest element in the scene. The ratio of tree height to the tree diameter (the finest scale in our simulations) is used. Figs. 15 and 16 show measured and predicted BRFs and their correlation for the SSAOJP and SSAOA sites. In these examples, the simulations compare well with the field data.

6. Conclusions

Analytical and Monte Carlo generated models of the pair correlation function have been developed. Given two horizontal

planes in the vegetation canopy, this function describes the correlation between foliated points on these planes as a function of the horizontal distance. Its derivative at the origin is diagnostic of the essential variability of canopy structure at the finest scale. For two points separated by a short distance, values of the conditional pair correlation function are close to one. This is the effect of clumping of foliage elements; that is, detecting a leaf makes it more likely that the next leaf will be detected nearby. At distances comparable to the crown horizontal size the conditional pair correlation function reaches its minimum. With further increase in the horizontal distance, it tends to a constant value and then levels off. This constant value is the probability of finding a foliated point on the horizontal plane at a given depth. Beyond a distance at which the correlation function saturates, there is no relation between foliated points.

The stochastic 1D radiative transfer equations capture the effects of the 3D canopy structure on the canopy reflective and absorptive properties. Ignoring the canopy structure can result in an underestimation of the canopy transmittance at the expense of overestimation of the canopy absorptance and reflectance. Transmittance, reflectance and absorptance of the 3D vegetation canopy vary with canopy LAI at a slower rate than 1D model can possibly predict. Ignoring this fact in interpretation of satellite data can lead to overestimation of the saturation domain, i.e., a range of canopy reflectance values which are insensitive to variation in canopy structure. The stochastic radiative transfer equations reproduce the effect of sunlit areas of the underlying surface on the canopy leaving radiation. They adequately account for impact of canopy structure on relationships between NDVI, LAI and canopy absorptance. Our analysis suggests that the foliage spatial correlation is primarily responsible for these effects. The pair correlation function, therefore, is the most natural and physically meaningful measure of canopy variability over a wide range of scales.

Simulations are compared with the PARABOLA measurements from two forest sites to evaluate the model performance. The sites include coniferous and broadleaf forest stands in the BOREAS Southern Study Areas. The pair correlation function was parameterized with tree structural parameters available from field campaigns conducted at these sites. The overall agreement between the modeled and measured canopy reflectances is very good.

To summarize, the stochastic 1D radiative transfer equations provide a powerful tool to develop operational algorithms for monitoring 3D canopy structure from space because (i) its solution coincides exactly with what satellite-borne sensors measure; that is, the mean intensity emanating from the smallest area to be resolved, from a pixel; (ii) it accounts for 3D effects through a small set of well defined measurable parameters; and (iii) it is as simple as the conventional 1D radiative transfer equation.

Acknowledgment

This research was funded by the National Aeronautics and Space Administration (NASA) through MODIS contracts NAS5-

96061, NNG04HZ09C, the Jet Propulsion Laboratory, California Institute of Technology under MISR contract 1259071, and by the NASA National Polar Orbiting Operational Environmental Satellite System Preparatory Project (NPP) under Grant NNG04GI52G. We gratefully acknowledge this support.

Appendix A. Stochastic radiative transfer equations

The indicator function approach is based on the following equation for the statistical closure (Shabanov et al., 2000; Titov, 1990; Vainikko, 1973)

$$\frac{\langle \int_S \gamma(r_z) \gamma(r_z - \ell \Omega) I(r_z - \ell \Omega, \Omega) dx dy \rangle}{S} = q(z, \xi, \Omega) U(\xi, \Omega). \quad (\text{A1})$$

Titov (1990) showed that this approximation to the second moment is accurate if a stationary Poisson point process is used to derive the indicator function γ (Appendix C). Here U and q are defined by Eqs. (2) and (4), and $\langle \cdot \rangle$ denotes ensemble averaging, i.e., over all possible realizations of the indicator function γ within a satellite pixel S . The notations and coordinate systems for spatial and directional variables are introduced in Fig. 2.

Under the assumptions formulated in Section 2, the horizontal average intensity $\bar{I}(z, \Omega)$ for downward ($\mu = \cos \theta < 0$) and upward ($\mu = \cos \theta > 0$) directions at depth z can be expressed via the second moment $U(z, \Omega)$ of the 3D radiation field as (Shabanov et al., 2000; Vainikko, 1973)

$$|\mu| \bar{I}(z, \Omega) = - \int_0^z \sigma(\Omega) p(\xi) U(\xi, \Omega) d\xi + \int_0^z p(\xi) S(\xi, \Omega) d\xi + |\mu| \bar{I}_0(\Omega), \quad \mu < 0, \quad (\text{A2a})$$

$$|\mu| \bar{I}(z, \Omega) = - \int_z^H \sigma(\Omega) p(\xi) U(\xi, \Omega) d\xi + \int_z^H p(\xi) S(\xi, \Omega) d\xi + |\mu| \bar{I}_H(\Omega), \quad \mu > 0, \quad (\text{A2b})$$

Here $\sigma(\Omega) = d_L G(\Omega)$ is the total interaction cross section (extinction coefficient), d_L is the leaf area volume density, $G(\Omega)$ is the geometry factor (Knyazikhin et al., 2005a; Oker-Blom & Smolander, 1988; Ross, 1981; Stenberg, 1998). The probability, $p(z)$, of finding a foliated point at depth z is defined by Eq. (3).

The scattering integral $S(\xi, z)$ has the following form

$$S(\xi, \Omega) = \int_{4\pi} \sigma_s(\Omega' \rightarrow \Omega) U(\xi, \Omega') d\Omega'.$$

Here 4π denotes the unit sphere, $\sigma_s(\Omega' \rightarrow \Omega) = d_L \pi^{-1} \Gamma(\Omega' \rightarrow \Omega)$ is the differential scattering coefficient and $\Gamma(\Omega' \rightarrow \Omega)$ is the area scattering phase function (Knyazikhin et al., 2005a; Ross, 1981). Finally, \bar{I}_0 and \bar{I}_H are mean intensities of radiation penetrating into the canopy through upper ($z=0$) and lower ($z=H$) boundaries, respectively.

The second moment $U(z, \Omega)$ satisfies the following integral equations

$$|\mu| U(z, \Omega) = - \int_0^z \sigma(\Omega) K(z, \xi, \Omega) U(\xi, \Omega) d\xi + \int_0^z K(z, \xi, \Omega) S(\xi, \Omega) d\xi + |\mu| U_0(z, \Omega), \quad \mu < 0, \quad (\text{A3a})$$

$$|\mu| U(z, \Omega) = - \int_z^H \sigma(\Omega) K(z, \xi, \Omega) U(\xi, \Omega) d\xi + \int_z^H K(z, \xi, \Omega) S(\xi, \Omega) d\xi + |\mu| U_H(z, \Omega), \quad \mu > 0. \quad (\text{A3b})$$

Here $K(z, \xi, \Omega)$ is the conditional pair correlation function, $K(z, \xi, \Omega) = q(z, \xi, \Omega) / p(z)$. The second moments of downward, $U_0(z, \Omega)$, and upward, $U_H(z, \Omega)$, radiation penetrating into the canopy through the upper and lower boundaries are defined as

$$U_0(z, \Omega) = \frac{\langle \int_S \gamma(r_z) I(r_z - \ell_0 \Omega) dx dy \rangle}{\langle \int_S \gamma(r_z) dx dy \rangle}, \quad \mu < 0, \quad (\text{A4})$$

$$U_H(z, \Omega) = \frac{\langle \int_S \gamma(r_z) I(r_z - \ell_H \Omega) dx dy \rangle}{\langle \int_S \gamma(r_z) dx dy \rangle}, \quad \mu > 0,$$

where $r_z = (x, y, z)$ is a point on the plane z (Fig. 2); ℓ_0 (ℓ_H) is the distance between r_z and the upper (lower) boundary along the direction $-\Omega$. For the horizontally homogeneous incoming radiation, $U_0(z, \Omega) = \bar{I}_0(\Omega)$ and $U_H(z, \Omega) = \bar{I}_H(\Omega)$. In this case, the equations for $\bar{I}(z, \Omega)$ and $U(z, \Omega)$ derived by averaging the three-dimensional radiative transfer equation over space and the ensemble of canopy realizations coincide; that is, the radiation field is ergodic (Titov, 1990).

Appendix B. Some properties of the stochastic radiative transfer equations

1. The mean intensity, $\bar{U}(z, \Omega)$, accumulated over non-foliated points at depth z is

$$\bar{U}(z, \Omega) = \frac{\langle \int_S I(x, y, z, \Omega) [1 - \gamma(x, y, z)] dx dy \rangle}{\langle \int_S [1 - \gamma(x, y, z)] dx dy \rangle}. \quad (\text{B1})$$

It follows from Eqs. (1–3 and A1) that

$$\bar{I}(z, \Omega) = p(z) U(z, \Omega) + (1 - p(z)) \bar{U}(z, \Omega). \quad (\text{B2})$$

2. The mean up- and downward radiation flux densities accumulated over foliated, $F_f^{\uparrow \downarrow}(z)$, non-foliated, $F_U^{\uparrow \downarrow}(z)$, and all points, $F_j^{\uparrow \downarrow}(z)$, at depth z are defined as

$$F_j^{\uparrow \downarrow}(z) = \frac{1}{i_0 |\mu_0|} \int_{2\pi\pi} J(z, \Omega) |\mu| d\Omega. \quad (\text{B3})$$

Here $J(z, \Omega)$ represents either $U(z, \Omega)$, $\bar{U}(z, \Omega)$ or $\bar{I}(z, \Omega)$, i_0 is the intensity of the incident radiation; μ_0 and μ are cosines of the solar zenith angle and the polar angle of the direction Ω ,

respectively; $2\pi^-$ ($2\pi^+$) denotes the downward (upward) hemisphere of directions. It follows from Eq. (B2) that

$$F_I^{\downarrow\uparrow}(z) = p(z)F_U^{\downarrow\uparrow}(z) + (1 - p(z))F_V^{\downarrow\uparrow}(z). \quad (\text{B4})$$

3. Let leaves be spatially uncorrelated, i.e., $q(z, \xi, \Omega) = p(z)p(\xi)$, and the incoming radiation be horizontally homogeneous, i.e., $U_0(z, \Omega) = \bar{I}_0(\Omega)$ and $U_H(z, \Omega) = \bar{I}_H(\Omega)$. Subtracting Eqs. (A3a) and (A3b) from Eqs. (A2a) and (A2b), one obtains $\bar{I}(z, \Omega) - U(z, \Omega) = 0$. Differentiating Eqs. (A3a) and (A3b) with respect to z , the stochastic radiative transfer equation for the second moment rearranges to the standard boundary value problem for 1D radiative transfer equation with the extinction coefficient $\sigma(z, \Omega) = d_L p(z)G(\Omega)$ and the differential scattering coefficient $\sigma_s(\Omega' \rightarrow \Omega) = d_L p(z)\pi^{-1}\Gamma(\Omega' \rightarrow \Omega)$.

4. Consider a 3D vegetation canopy consisting of identical cylindrical in shape trees. The probability $p(z)$ is constant and coincides with the ground cover, i.e., $p(z) = g$. It is convenient to express the vertical coordinate in terms of the normalized depth, $\bar{z} = z/H$ (dimensionless). The normalized depth varies between 0 (canopy top) and 1 (canopy bottom). The extinction and differential scattering coefficients in the stochastic radiative transfer Eqs. (A2a) (A2b) (A3a) (A3b) rearrange to $\sigma(z, \Omega) = L_0 G(\Omega)$ and $\sigma_s(\Omega' \rightarrow \Omega) = L_0 \pi^{-1} \Gamma(\Omega' \rightarrow \Omega)$ where $L_0 = d_L H$ is the plant leaf area index. If leaf are not spatially correlated, i.e., $K(z, \xi, \Omega) = g$, the stochastic radiative transfer equations reduce to the conventional 1D radiative transfer equation with the extinction coefficient $\sigma(z, \Omega) = \text{LAI} \cdot G(\Omega)$ and the differential scattering coefficient $\sigma_s(\Omega' \rightarrow \Omega) = \text{LAI} \cdot \pi^{-1} \Gamma(\Omega' \rightarrow \Omega)$ where $\text{LAI} = gL_0$ is the canopy leaf area index. Thus, solution to the stochastic radiative transfer equations depend on the product gL_0 but not on absolute values of g and L_0 in this case.

Appendix C. Analytical models of the pair correlation function

The stochastic geometry provides a powerful tool to derive pair correlation functions. We will follow the Boolean model of random set to simulate 3D canopy structure. Below, the formulation of Stoyan et al. (1995) is adopted.

Consider points scattered on the horizontal plane according to a stationary Poisson point process of intensity d . Since the intensity gives the mean number of points to be found in a unit area, this parameter can be treated as the stem density. On each of these points a geometrical figure is placed. The union of all of these figures is the stochastic model of the canopy structure. The geometrical figure is assumed to be a vertical solid, i.e., a volume obtained by rotating a curve about the vertical axis. Its horizontal cross section at depth z is a circle of the depth dependent radius $r(z)$. We shall restrict our consideration to vegetation canopies consisting of identical trees.

Let T_z be a set of crown cross sections at depth z projected onto a reference horizontal plane, say, $z=0$. This set consists of identical circles of the radius $r(z)$. The pair correlation function,

$q(z, \xi, \lambda)$, can be determined in terms of measures of the overlap between two sets, T_z and $T_\xi - \lambda \mathbf{u}$, i.e.,

$$q(z, \xi, \lambda) = \Pr(a \in T_z \text{ and } b \in T_\xi) = E[\text{mes}(T_z \cap T_\xi - \lambda \mathbf{u})]. \quad (\text{C1})$$

Here a, b and \mathbf{u} are projections of points r_z and $r_\xi = r_z - \mathcal{L}\Omega$ (Fig. 2) and the vector Ω onto the reference plane, respectively; $T_\xi - \lambda \mathbf{u}$ is the set T_ξ shifted by an increment λ along the direction \mathbf{u} ; $\text{mes}(A)$ denotes the Lebesgue measure (area) of a set A on the reference plane; and $E(A)$ stands for the mean fraction $A \cap B$ occupied by A in a region B of unit area, $\text{mes}(B) = 1$. Thus, the generation of 3D canopy structure can be reduced to Boolean models of random sets on the horizontal plane. Fig. 4 shows examples of the conditional pair correlation function, $K(z, \xi, \lambda) = q(z, \xi, \lambda)/p(z)$, of the Poisson germ-grain, Matérn cluster and Matérn hard-core processes. Their short descriptions are given below.

1. *Poisson germ-grain models.* In the above formulation of the stochastic model, the points of the Poisson process are germs of the model while the crown cross sections are the primary grains. The primary grains are represented by discs of the radius $r(z)$ and $r(\xi)$. Following derivations of the above cited monograph on p. 68, the covariance function (C1) takes the following form

$$q(z, \xi, \lambda) = p(z) + p(\xi) - 1 + [1 - p(z)][1 - p(\xi)] \exp\{d\theta(z, \xi, \lambda)\}, \quad (\text{C2a})$$

$$p(z) = 1 - \exp\{-d\pi r^2(z)\}. \quad (\text{C2b})$$

Here $p(z)$ is defined by Eq. (3) and, for $r(\xi) \geq r(z)$,

$$\theta(z, \xi, \lambda) = \begin{cases} \pi r^2(z), & \text{if } r(\xi) - r(z) > \lambda, \\ 0, & \text{if } r(\xi) + r(z) \leq \lambda, \\ \alpha r^2(z) + \beta r^2(\xi) - \lambda r(\xi) \sin \alpha, & \text{otherwise,} \end{cases} \quad (\text{C2c})$$

$$\alpha = \arccos\left(\frac{r^2(\xi) - r^2(z) + \lambda^2}{2\lambda r(\xi)}\right), \quad \beta = \arccos\left(\frac{r^2(z) - r^2(\xi) + \lambda^2}{2\lambda r(z)}\right). \quad (\text{C2d})$$

For $r(\xi) < r(z)$, $\theta(z, \xi, \lambda) = \theta(\xi, z, \lambda)$.

For cylindrical in shape trees, $p(z) = g$, $r(\xi) = r(z) = D_B/2$, $\alpha = \beta = \arccos(\lambda/D_B)$. It follows from Eqs. (C2a)–(C2d) that the pair correlation function depends on the horizontal distance λ normalized by the crown base diameter D_B , i.e.,

$$q(\lambda) = 2g - 1 + (1 - g)^{2 - \kappa(\lambda, D_B)}. \quad (\text{C3a})$$

The coefficient $\kappa(\lambda, D_B)$ is an area occupied by the intersection of two circles of the radius D_B shifted by a distance λ normalized by the circle area $\pi D_B^2/4$, i.e.,

$$\kappa(\lambda, D_B) = 2\pi^{-1} \left[\arccos \frac{\lambda}{D_B} - \frac{\lambda}{D_B} \sqrt{1 - \left(\frac{\lambda}{D_B}\right)^2} \right] \mathcal{H}(D_B - \lambda), \quad (\text{C3b})$$

where $H(s)$ is the Heaviside function. The derivative at the origin $\lambda=0$ is

$$\left. \frac{dq(\lambda)}{d\lambda} \right|_{\lambda=0} = \frac{4(1-g)\ln(1-g)}{\pi D_B}. \quad (C4)$$

2. *Matérn cluster process*. Cluster point processes are produced from the stationary Poisson point process of intensity d by replacing each point with a representative cluster C_0 of points. The representative cluster is a point process. The number of points in C_0 has a Poisson distribution with the positive parameter \bar{m} . The points of C_0 are independently and uniformly scattered in the circle of the diameter $D_0=2r_0$. On each of these points a geometrical figure (clump) is placed. The union of all of these figures is the stochastic cluster model of random sets on the horizontal plane. For clumps represented by circles with the diameter $D_c=2r_c$, the pair correlation function can be factorized into probabilities of finding two points in the clusters and finding clumps at these points, i.e.,

$$q(\lambda) = [2g_c - 1 + (1 - g_c)^{2-\kappa(\lambda, D_c)}][2g_0 - 1 + (1 - g_0)^{2-\kappa(\lambda, D_0)}],$$

$$g_c = 1 - \exp(-\bar{m}\pi r_c^2), \quad g_0 = 1 - \exp(-d\pi r_0^2).$$

The probability, $p(z)$, of finding a foliated point at depth z is given by $p(z)=g_c g_0$.

3. *Matérn hard-core model*. Tree crowns in the above models can be intersected forming complex configuration. The hard-core models describe patterns produced by the locations of centers of non-overlapping circles of a given radius. Consider the Matérn hard-core point process (Stoyan et al., 1995) which is produced from a stationary Poisson point process of intensity d by deleting points satisfying some definite rules. Consider a vegetation canopy consisting of cylindrical in shape trees. Let $v=\pi D_B^2$ where D_B is the crown base diameter. The intensity, d_{HC} , and the second order product density, $\rho^{(2)}(\lambda)$, of the Matérn hard-core point process are given by (Stoyan et al., 1995)

$$d_{HC} = \frac{1 - \exp(-dv)}{v}, \quad (C5)$$

$$\rho^{(2)}(\lambda) = \frac{2\Gamma(\lambda)[1 - \exp(-dv)] - 2v[1 - \exp(-d\Gamma(\lambda))]}{v\Gamma(\lambda)[\Gamma(\lambda) - v]} \mathcal{H}(\lambda - D_B), \quad (C6)$$

$$\Gamma(\lambda) = v[2 - \kappa(\lambda, 2D_B)]. \quad (C7)$$

The second moment $\rho^{(2)}(\lambda)$ can be interpreted as the probability density that two tree centers are separated by the distance λ .

Since the trees are not overlapped, the ground cover is $g=d_{HC}\pi D_B^2/4=d_{HC}v/4$. The pair correlation function is decomposed into the sum of probabilities of finding foliated points in the same crown and in different crowns, i.e.,

$$q(\lambda) = g\kappa(\lambda, D_B) + \int \frac{\|\mathbf{v}\| \leq D_B}{\|\mathbf{v}'\| \leq D_B} \rho^{(2)}(\|\mathbf{v} - \mathbf{v}' + \lambda \mathbf{u}\|) d\mathbf{v}d\mathbf{v}', \quad (C8)$$

where $\mathbf{u}=(0,1)$ is the unit vector on the plane $z=0$ and $\|\cdot\|$ is the Euclidean distance. Note the second order product density, $\rho^{(2)}(\lambda)$, does not depend on \mathbf{u} .

References

- Asrar, G., Fuchs, M., Kanemasu, E. T., & Hatfield, J. L. (1984). Estimating absorbed photosynthetic radiation and leaf area index from spectral reflectance in wheat. *Agronomy Journal*, 76, 300–306.
- Asrar, G., Myneni, R. B., & Choudhury, B. J. (1992). Spatial heterogeneity in vegetation canopies and remote sensing of absorbed photosynthetically active radiation: A model study. *Remote Sensing of Environment*, 41, 85–103.
- Bothwell, G. W., Hansen, E. G., Vargo, R. E., & Miller, K. C. (2002). The multi-angle imaging spectroradiometer science data system, its products, tools, and performance. *IEEE Transactions on Geoscience and Remote Sensing*, 40, 1467–1476.
- Buermann, W., Dong, J., Zeng, X., Myneni, R. B., & Dickinson, R. E. (2001). Evaluation of the utility of satellite based vegetation leaf area index data for climate simulations. *Journal of Climate*, 14(17), 3536–3550.
- Byrne, N. (2005). Three-dimensional radiative transfer in stochastic media. In A. Marshak & A. B. Davis (Eds.), *Three dimensional radiative transfer in the cloudy atmosphere* (pp. 385–424). Springer-Verlag.
- Castel, T., Beaudoin, A., Flourey, N., Le Toan, T., Caraglio, Y., & Barczi, J. F. (2001). Deriving forest canopy parameters for backscatter models using the AMAP architectural plant model. *IEEE Transactions on Geoscience and Remote Sensing*, 39(3), 571–583.
- Chen, J. M. (1996). Optically-based methods for measuring seasonable variation of leaf area index in boreal conifer stands. *Agricultural and Forest Meteorology*, 80, 135–163.
- Chen, J. M., & Leblanc, S. G. (1997). A four-scale bidirectional reflectance model based on canopy architecture. *IEEE Transactions on Geoscience and Remote Sensing*, 35, 1316–1337.
- Chen, R., Jupp, D. L. B., & Woodcock, C. E. (1993). Nonlinear estimation of scene parameters from digital images using zero-hit run-length statistics. *IEEE Transactions on Geoscience and Remote Sensing*, 31(3), 735–746.
- Davis, A. B., & Knyazikhin, Y. (2005). A primer in three-dimensional radiative transfer. In A. Marshak & A. B. Davis (Eds.), *Three Dimensional Radiative Transfer in the Cloudy Atmosphere* (pp. 153–242). Springer-Verlag.
- Deering, D. W., Eck, T. F., & Banerjee, B. (1999). Characterization of the reflectance anisotropy of three boreal forest canopies in spring–summer. *Remote Sensing of Environment*, 67, 205–229.
- Deering, D. W., & Leone, P. (1986). A sphere scanning radiometer for rapid directional measurements of sky and ground radiance. *Remote Sensing of Environment*, 19, 1–24.
- Diner, D. J., Asner, G. P., Davies, R., Knyazikhin, Y., Muller, J. P., Nolin, A. W., et al. (1999). New directions in Earth observing: Scientific application of multi-angle remote sensing. *Bulletin of the American Meteorological Society*, 80(11), 2209–2228.
- Hardy, J. P., Davis, R. E., Jordan, R., Ni, W., & Woodcock, C. (1998). Snow ablation modeling in a mature aspen stand of the boreal forest. *Hydrological Processes*, 12, 1763–1778.
- Huang, D., Knyazikhin, Y., Dickinson, R. E., Rautiainen, M., Stenberg, P., Disney, M., et al. (2007). Canopy spectral invariants for remote sensing and model applications. *Remote Sensing of Environment*, 106, 106–122.
- Huete, A., Didan, K., Miura, T., Rodriguez, E. P., Gao, X., & Ferreira, L. G. (2002). Overview of the radiometric and biophysical performance of the MODIS vegetation indices. *Remote Sensing of Environment*, 83, 195–213.
- Jupp, D. L., Strahler, A. H., & Woodcock, C. E. (1988). Autocorrelation and regularization in digital images I. Basic theory. *IEEE Transactions on Geoscience and Remote Sensing*, 26(4), 463–473.
- Jupp, D. L., Strahler, A. H., & Woodcock, C. E. (1989). Autocorrelation and regularization in digital images II. Simple image models. *IEEE Transactions on Geoscience and Remote Sensing*, 27(3), 247–258.
- Justice, C. O., Townshend, J. R. G., Vermote, E. F., Masuoka, E., Wolfe, R. E., Saleous, N., et al. (2002). An overview of MODIS land data processing and product status. *Remote Sensing of Environment*, 83, 3–15.

- Justice, C. O., Vermote, E., Townshed, J. R. G., Defries, R., Roy, D. P., Hall, D. K., et al. (1998). The moderate resolution imaging spectroradiometer (MODIS): Land remote sensing for global research. *IEEE Transactions on Geoscience and Remote Sensing*, 36, 1228–1249.
- Kaufmann, R. K., Zhou, L., Knyazikhin, Y., Shabanov, N. V., Myneni, R. B., & Tucker, C. J. (2000). Effect of orbital drift and sensor changes on the time series of AVHRR vegetation index data. *IEEE Transactions on Geoscience and Remote Sensing*, 38(6), 2584–2597.
- Knyazikhin, Y., Kranigk, J., Myneni, R. B., Panfyorov, O., & Gravenhorst, G. (1998). Influence of small-scale structure on radiative transfer and photosynthesis in vegetation cover. *Journal of Geophysical Research*, 103(DD6), 6133–6144.
- Knyazikhin, Y., Marshak, A., Larsen, M., Wiscombe, W. J., Martonchik, J. V., & Myneni, R. B. (2005). Small-scale drop size variability: Impact on estimation of cloud optical properties. *Journal of the Atmospheric Sciences*, 62(7), 2555–2567.
- Knyazikhin, Y., Marshak, A., & Myneni, R. B. (2005). Three-dimensional radiative transfer in vegetation canopies and cloud-vegetation interaction. In A. Marshak & A. B. Davis (Eds.), *Three dimensional radiative transfer in the cloudy atmosphere* (pp. 617–652). Springer-Verlag.
- Knyazikhin, Y., Martonchik, J. V., Myneni, R. B., Diner, D. J., & Running, S. W. (1998). Synergistic algorithm for estimating vegetation canopy leaf area index and fraction of absorbed photosynthetically active radiation from MODIS and MISR data. *Journal of Geophysical Research*, 103, 32257–32274.
- Kotchenova, S. Y., Shabanov, N. V., Knyazikhin, Y., Davis, A. B., Dubayah, R., & Myneni, R. B. (2003). Modeling lidar with time-dependent stochastic radiative transfer theory for remote estimation of forest structure. *Journal of Geophysical Research*, 108, 17539–17549 (Art. No. 4484).
- Larsen, D. R., & Kersaw, J. A., Jr. (1996). Influence of canopy structure assumptions on prediction from Beer's law. A comparison of deterministic and stochastic simulations. *Agricultural and Forest Meteorology*, 81, 61–77.
- Martonchik, J. V., Bruegge, C. J., & Strahler, A. (2000). A review of reflectance nomenclature used in remote sensing. *Remote Sensing Reviews*, 19, 9–20.
- Middleton, E., & Sullivan, J. (2000). *BOREAS TE-10 Leaf Optical Properties for SSA Species*. Data set. Available on-line [<http://www.daac.ornl.gov>] from Oak Ridge National Laboratory Distributed Active Archive Center, Oak Ridge, Tennessee, U.S.A.
- Miller, J. R., White, H. P., Chen, J. M., Peddle, D. R., McDermid, G., Fomier, R. A., et al. (1997). Seasonal change in understory reflectance of boreal forests and influence on canopy vegetation indices. *Journal of Geophysical Research*, 102(D24), 29,729–29,736.
- Myneni, R. B. (1991). Modeling radiative transfer and photosynthesis in three-dimensional vegetation canopies. *Agricultural and Forest Meteorology*, 55, 323–344.
- Myneni, R. B., Hall, F. G., Sellers, P. J., & Marshak, A. L. (1995). The interpretation of spectral vegetation indexes. *IEEE Transactions on Geoscience and Remote Sensing*, 33, 481–486.
- Ni, W., Li, X., Woodcock, C. E., Roujean, J. L., & Davis, R. E. (1997). Transmission of solar radiation in boreal conifer forests: Measurements and models. *Journal of Geophysical Research*, 102(D24), 29,555–29,566.
- Nilson, T. (1999). Inversion of gap frequency data in forest stands. *Agricultural and Forest Meteorology*, 98–99, 437–448.
- Oker-Blom, P., & Smolander, H. (1988). The ratio of shoot silhouette area to total needle area in Scots pine. *Forest Science*, 34, 894–906.
- Pomraning, G. C. (1991). *Linear kinetic theory and particle transport in stochastic mixtures* (pp. 235). New Jersey: World Scientific.
- Pomraning, G. C. (1996). Transport theory in discrete stochastic mixtures. *Advances in Nuclear Science and Technology*, 24, 47–93.
- Ranson, K. J., Sun, G., Weishampel, J. F., & Knox, R. G. (1997). Forest biomass from combined ecosystem and radar backscatter modeling. *Remote Sensing of Environment*, 59, 118–133.
- Rautiainen, M., & Stenberg, P. (2005). Application of photon recollision probability in coniferous canopy reflectance model. *Remote Sensing of Environment*, 96, 98–107.
- Ross, J. (1981). *The radiation regime and architecture of plant stands* (pp. 391). Norwell, MA: Dr. W. Junk.
- Roujean, J. L. (1999). Two-story equations of transmission of solar energy (TESTSE) in open boreal conifer tree stands. *Journal of Geophysical Research*, 104(D22), 27,869–27,879.
- Roujean, J. L. (1999). Measurements of PAR transmittance within boreal forest stands during BOREAS. *Agricultural and Forest Meteorology*, 93, 1–6.
- Schaaf, C. B., Gao, F., Strahler, A. H., Lucht, W., Li, X., Tsang, T., et al. (2002). First operational BRDF, Albedo and Nadir reflectance products from MODIS. *Remote Sensing of Environment*, 83, 135–148.
- Sellers, P. J., Randall, D. A., Betts, A. K., Hall, F. G., Berry, J. A., Collatz, G. J., et al. (1992). Modeling the exchanges of energy, water, and carbon between continents and the atmosphere. *Science*, 275, 502–509.
- Shabanov, N. V., Knyazikhin, Y., Baret, F., & Myneni, R. B. (2000). Stochastic modeling of radiation regime in discontinuous vegetation canopies. *Remote Sensing of Environment*, 74(1), 125–144.
- Shabanov, N. V., Kotchenova, S., Huang, D., Yang, W., Tan, B., Knyazikhin, Y., et al. (2005). Analysis and optimization of the MODIS leaf area index algorithm retrievals over broadleaf forests. *IEEE Transactions on Geoscience and Remote Sensing*, 43(8), 1855–1865.
- Smolander, S., & Stenberg, P. (2003). A method to account for shoot scale clumping in coniferous canopy reflectance models. *Remote Sensing of Environment*, 88, 363–373.
- Smolander, S., & Stenberg, P. (2005). Simple parameterizations of the radiation budget of uniform broadleaved and coniferous canopies. *Remote Sensing of Environment*, 94, 355–363.
- Stenberg, P. (1996). Simulations of the effect of shoot structure and orientation on vertical gradients in intercepted light by conifer canopies. *Tree Physiology*, 16, 99–108.
- Stenberg, P. (1998). Implications of shoot structure on the rate of photosynthesis at different levels in a coniferous canopy using a model incorporating grouping and penumbra. *Functional Ecology*, 12, 82–91.
- Stoyan, D., Kendall, S. W., & Mecke, J. (1995). *Stochastic geometry and its application* (pp. 436). New York: John Wiley & Sons.
- Strahler, A. H., & Jupp, D. L. B. (1990). Modeling bidirectional reflectance of forests and woodlands using Boolean models and geometric optics. *Remote Sensing of Environment*, 34, 153–160.
- Titov, G. A. (1990). Statistical description of radiation transfer in clouds. *Journal of the Atmospheric Sciences*, 47, 24–38.
- Tucker, C. J. (1979). Red and photographic infrared linear combination for monitoring vegetation. *Remote Sensing of Environment*, 8, 127–150.
- Tucker, C. J., Fung, Y., Keeling, C. D., & Gammon, R. H. (1986). Relationship between atmospheric CO₂ variations and a satellite-derived vegetation index. *Nature*, 319, 195–199.
- Vainikko, G. M. (1973). Transfer approach to the mean intensity of radiation in non-continuous clouds. *Trudy MGK SSSR. Meteorological Investigations*, 21, 28–37.